

Knotting of random ring polymers in confined spaces

C. Micheletti¹, D. Marenduzzo², E. Orlandini³, D. W. Sumners⁴

¹ *International School for Advanced Studies (SISSA)*

and INFN, via Beirut 2-4, 34100 Trieste, Italy

² *Mathematics Institute, University of Warwick, Coventry, CV4 7AL, UK*

³ *Dipartimento di Fisica and Sezione INFN,*

Università di Padova, Via Marzolo 8, 35121 Padova, Italy

⁴ *Department of Mathematics, Florida State University, Tallahassee, FL 32306, USA*

Abstract

Stochastic simulations are used to characterize the knotting distributions of random ring polymers confined in spheres of various radii. The approach is based on the use of multiple Markov chains and reweighting techniques, combined with effective strategies for simplifying the geometrical complexity of ring conformations without altering their knot type. By these means we extend previous studies and characterize in detail how the probability to form a given prime or composite knot behaves in terms of the number of ring segments, N , and confining radius, R . For $50 \leq N \leq 450$ we show that the probability of forming a composite knot rises significantly with the confinement, while the occurrence probability of prime knots are, in general, non-monotonic functions of $1/R$. The dependence of other geometrical indicators, such as writhe and chirality, in terms of R and N is also characterized. It is found that the writhe distribution broadens as the confining sphere narrows.

I. INTRODUCTION

In recent years, novel motivations to characterize the properties of knotted ring polymers have been provided by *in vivo* and *in vitro* experiments on molecules of biological interest. Quantitative estimates for the occurrence of various types of knots are particularly abundant for the case of circular DNA, which can be manipulated and probed by a variety of physico-chemical techniques, such as gel electrophoresis and others (see e.g. Ref. [1, 2, 3]). The available data provides crucial benchmarks for theoretical models aimed at describing the occurrence of knots in biomolecules. These models, in turn, allow us to elucidate the existence and functionality of cellular machinery designed to alter the topology of circular DNA *in vivo*. For example, due to the action of topoisomerase II enzyme [4, 5], it is known that the fraction of knotted plasmid DNA *in vivo* (wild-type *E. Coli*) is much smaller than the statistical equilibrium value predicted theoretically [2]. Besides the occurrence of knots in DNA molecules that are free in solution another biologically relevant case is the presence of knots in tightly-packed DNA, such as that confined in viral capsids [6, 7, 8, 9, 10, 11]. For example, recent experimental investigations have revealed that the probability of occurrence of cyclised knotted DNA is very high inside the T4 deletion mutant viral capsid [6]. The experimental characterization was accompanied by numerical simulations where a DNA molecule was schematized as a phantom (i.e. interpenetrable) ring which suggested that the observed high knotting probability was likely to be a passive consequence of the spatial confinement, rather than to be due to active biological mechanisms [6]. In this work we extend the previous studies [6, 12, 13, 14] not only by considerably extending the length and degree of confinement of the rings, but also by using the entire array of knot invariants to identify the various types of occurring knots. This is accomplished by first using a powerful statistical mechanical framework for the efficient sampling of the ring conformations confined in tight spheres and, secondly, by simplifying the sampled ring conformations so as to aid their correct identification in spite of their initially very complex two-dimensional projections.

The techniques used in this study to overcome these problems are discussed in the next section. In sections 3 and 4 we present the results pertaining to the knotting of a confined phantom chain and to its writhe and chirality as it is confined in progressively smaller spheres. We also discuss the scaling laws of some knotting probabilities, and we map a diagram in which we identify the most populated knot type for a given length and confinement level. Section 5 contains a discussion of our results and our conclusions.

II. MODEL AND METHODS

At the heart of this study is the generation, by stochastic simulation, of uncorrelated configurations of random polymer rings of various length and enclosed in spheres of various radii. As customary, the ring is constituted by N segments of unit length; no self-avoidance is imposed on the ring. With reference to the origin of the embedding in three-dimensional Euclidean space, each ring conformation, Γ , is described by the coordinates of the vertices, $\Gamma \equiv \{\vec{r}_1, \vec{r}_2, \vec{r}_N, \vec{r}_{N+1} \equiv \vec{r}_1\}$. To each ring configuration we associate a radius $R(\Gamma)$, defined as $R = \max_i |\vec{r}_i|$ which measures the distance from the origin of the vertex that is farthest from the origin itself. Obviously, a ring Γ can be enclosed only in spheres having radius larger than $R(\Gamma)$. This ensemble is therefore different from the one where the centre of the enclosing sphere is chosen to coincide with the geometrical centre of the ring. Although this second alternative is also intuitive and natural, the ensemble chosen here seems most naturally related to the experimental situation where one has the hull (e.g. a viral capsid) fixed in space and the enclosed molecule occupying any internal region.

We aim at calculating, for any given ring length, N , the number density of ring conformations of given knot type, K , that are generated by random sampling from the ensemble and can be accommodated inside a sphere of radius R . This quantity will be indicated as $W_N(K, R)$. A technique based on multiple Markov chains and histogram reweighting will be used to determine $W_N(K, R)$ up to a multiplicative constant [10, 15, 16]. The value of this constant is irrelevant for calculating the occurrence probability of various knots types (which is expressed in terms of suitable ratios of W_N terms, as discussed later).

In principle $W_N(K, R)$ could be obtained by an unbiased sampling of random ring conformations. In practice, the overwhelming majority of polymer rings will be “swollen”[17] and, therefore, an impractically long computing time would be necessary to accumulate reliable statistics for highly confined conformations. A more efficient alternative is to generate a succession of conformations picked with importance sampling criteria. At any stage of the procedure, one deforms the current ring conformation stochastically by moves preserving the chain connectivity and bond length. The usual Metropolis scheme is then employed to reject or accept newly-generated conformations based on the score assigned to them. In the simplest approach, the scoring function is chosen so as to penalize severely cases where a preassigned threshold value, \bar{R} is exceeded (while no penalty is introduced for configurations satisfying the hull constraint). Starting from an arbitrary conformation the stochastic evolution will eventually drive the system to configurations

that can fit inside the preassigned enclosing hull. However, this method also presents difficulties since, for the entropic reasons mentioned above, most of the sampled configurations will attain the maximum allowed value of R , that is \bar{R} . Their stochastic modification is therefore likely to produce a value for R that violates the hull constraint and hence leads to rejection. The large numbers of rejections encountered is such that impractically large number of MC steps are required to decorrelate the system as \bar{R} is decreased.

In the present study we reduce the impact of these sampling difficulties by two means. Rather than working in the ensemble of fixed \bar{R} , we work in the conjugated ensemble by introducing an auxiliary parameter, P , akin to the familiar “hydrostatic” pressure. For a given value of P and N , the number of *sampled* polymer rings having knot type K and radius equal to R is proportional to the weight $\exp(-P R)$ and to the number density of conformations having knot type K and radius equal to R , $\tilde{W}_N(K, R)$ (the logarithm of $\tilde{W}_N(K, R)$ provides the configurational entropy of the rings up to an additive constant):

$$n_N(K, R) \propto \tilde{W}_N(K, R) e^{-P R} \quad (1)$$

The tilde superscript is used to distinguish this quantity from the one introduced before which denoted the number density of conformations of given knot type that have radius less than or equal to R (as opposed to having exactly radius R). Since

$$W_N(K, \bar{R}) \propto \int_0^{\bar{R}} dR \tilde{W}_N(K, R) \quad (2)$$

we have

$$W_N(K, \bar{R}) \propto \int_0^{\bar{R}} dR n_N(K, R) e^{+P R} \quad (3)$$

At each value of P one can therefore reconstruct $W_N(K, R)$ throughout the range of explored values of R . As P is increased lower values of R are encountered. By optimally superimposing the $W_N(K, R)$ obtained at different values of P one can then recover the value of $W_N(K, R)$, for a continuous range of R spanning from the lowest to the largest observed values of R . The optimal superposition of the various W 's is carried out using the standard Ferrenberg-Swendsen approach. Once $W_N(K, R)$ is known, various quantities of interest can be calculated. For example, at given length, N , the expected fraction of polymer rings of knot type K that can fit inside a spheres of radius R is given by:

$$P_N(K, R) = \frac{W_N(K, R)}{\sum_{K'} W_N(K', R)} \quad (4)$$

where K' spans all knot types.

The reweighting procedure was used to produce most of the data presented here. The error in the quantities (4) and (6) is estimated from the semidispersion observed by applying the weighted histogram method separately to the first and second half of the polymer rings generated stochastically. Moreover the data pertaining to various “pressures” were not collected from independent runs, but by using the standard, yet powerful, multiple-Markov chains scheme. Within the latter framework all “replicas” of the system at the various pressures are run in parallel and, at times greater than the largest autocorrelation time, one proposes swaps of the ring conformations among two replicas at nearby pressure values. The swap is accepted according to a suitably-generalized Metropolis criterion [18]. The exchange of the replicas results in a significant decrease of the autocorrelation time in the system, and hence in a more effective sampling of the accessible conformational phase space.

The final focus of this section is the description of the strategy used to identify the type of knot associated to any given ring conformation. The classification of the knot type of a given ring conformation is facilitated by reducing the number of crossings in the knot diagram, while preserving knot type. Randomly generated rings, especially those confined in small spheres, typically present projections with a number of crossings that vastly exceeds the minimal one for that knot type. For example, unknotted conformations in rings of $N = 400$ segments confined in spheres of radius $R = 10$ typically present ~ 400 crossings. No general deterministic algorithm at present exists for obtaining minimal projections starting from a generic suboptimal one. A few stochastic methods have, however, been introduced that can simplify the initial diagram considerably. Our strategy to simplify the knot structure was based on a generalization of the techniques of refs. [19] and [20]. Starting from an initial conformation, we pick at random one vertex i and perform with equal probability one of the following two moves:

The first move consists of assigning a new position for i obtained as $\vec{x}_i^{new} = \alpha \vec{x}_i + (1 - \alpha)(\vec{x}_{i-1} + \vec{x}_{i+1})/2$, where α is a random number picked uniformly in the interval $[0.2, 0.8]$. The proposed new position is accepted only if the deformation of the chain when vertex i is moved continuously from the old to the new position does not lead to self-intersections of the ring. The repeated application of the operation leads to a smoothing and contraction of the initial chain and hence a simplification of the crossing pattern [20].

The second type of operation is an attempt to simplify the chain by removing vertex i . This can be viewed as a special case of the previous move where α is set equal to zero, i.e. vertex i is made collinear with the previous and following vertices. If this move is acceptable (in the same sense as before) then i is removed from the list of vertices.

The smoothing and shrinking operations are attempted until the number of vertices does not decrease in 10 successive system sweeps (a sweep consists in proposing either of the two elementary moves for a number of randomly chosen vertices equal to the ring length). Convergence is typically achieved in a dozen sweeps. This simplification procedure can reduce dramatically the number of crossings encountered in an arbitrary projection as shown in Fig. 1. For example, rings with $N = 400$ segments inside spheres of radius $R = 10$ are typically simplified down to rings with $N' \sim 35$ (non-equilateral) segments with projections having, on average, 30 crossings.

Of the simplified ring configurations we chose the projection with the minimum number of crossings produced by the smoothing scheme and encoded it in terms of the Dowker code [22] and then fed this code to the Knotfind programme [23]. The Knotfind programme then attempts to further reduce the number of crossings by performing modifications on the code (the modifications include some Reidemeister moves). The resulting knot representation is compared to a library of prime knot representations for correct identification. By these means it was possible to precisely identify prime knots (or prime components of composite knots) for prime and composite knots of up to 16 crossings. In some cases, even after the hierarchy of reduction of knot complexity, the diagrams could not be identified. This could reflect the genuine fact that the knot under consideration had a minimal projection with more than the threshold number of crossings (i.e. 16), or could simply reflect the inability to simplify it to a point where the knot projection had 16 or fewer crossings.

Whenever this situation is encountered the knot is classified as “unknown”. As visible in Fig. 2 the number of “unknown” knots grows with the decrease of the confining hull, R , as expected intuitively.

For the unconstrained case, $R = \infty$, the occurrence probability, $P_\tau(N)$ of various types of knots, τ , is shown in Fig. 3. The results appear consistent with previous studies [12, 19, 24, 25, 27] and the well known exponential decay [28, 29, 30, 31] of $P_\tau(N)$ as a function of N is verified for the simplest prime knots. In particular, by fitting of the unknot curve with the a single-exponential decay $P_\tau \propto \exp -(N/N_c)$ we obtain the decay length $N_c = 244 \pm 5$ which agrees quite well with the up-to-date independent estimates [26, 27].

III. RESULTS FOR CONFINED RINGS

We now discuss the case of random rings confined within a sphere of radius R . In Figs. 4a and 5a we show the unknotting probability as a function of inverse radius for rings of N segments. Besides the statistical error reflecting the finite sampling of knot configurations, the confidence in the curves for the occurrence probability is affected by the fraction of “unknown” knots, which may contain knots with crossing numbers less than or equal to 16, as well as knots with crossing numbers which exceed 16. As one moves towards smaller confining radii, the fraction of unknown knots becomes progressively higher, thus making uncertain the precise quantitative estimate of the occurrence of the various knot types. We use a threshold of 10% for the occurrence of unknown knots, $P_{unknown}$, in order to separate the reliable from the unreliable parts of the probability profiles. Moreover, no data are presented when $P_{unknown}$ exceeds 50%. To distinguish graphically these cases in Figs. 2- 4 the points falling in the region where $P_{unknown} > 0.1$ are denoted with open symbols. The reliable-unreliable boundary is instead shown as a red line on the two-dimensional probability surface of Fig. 5.

Different curves correspond to different values of N ranging from 50 up to 450 with incremental step $\Delta N = 25$. Note that, for fixed N , the unknotting probability remains fairly constant for $R > R_c$ (R_c is a length dependent threshold) and undergoes a pronounced decrease for $R < R_c$. For fixed R , the knotting probability decreases with N as expected. Michels and Wiegel, in their pioneering work [12], analysed the scaling properties of the unknotting probability for moderate values of N and confining radii, R , and suggested the following scaling form

$$\frac{P_{unknot}(N, \frac{1}{R})}{P_{unknot}(N, \frac{1}{R} = 0)} = g\left(\frac{N^\alpha}{R^3}\right), \quad (5)$$

where their estimate for the exponent α was 2.28. We have analysed our data, which span over much larger values of N and confining degree than ref. [12], and established that, though the scaling law of eqn. 5 remains valid, the exponent α is noticeably different from the previous estimate. The value of α providing the best collapse of the unknotting profiles for $N \geq 100$ was obtained from the procedure of refs. [32, 33] and resulted equal to $\alpha = 2.15 \pm 0.04$. The uncertainty on the exponent was estimated by dispersion of the optimal values of α leading to the curves collapse for two distinct sets of values of N . The quality of the obtained collapse is visible in Fig. 6.

Figs. 4b and 5b show, instead, the R dependence of the probability to observe a trefoil knot (P_{3_1}) for various lengths of the polymer ring. As for the unknotting probability there is a range of

R ($R > R_c$) for which P_{3_1} does not change too much with R . This “plateau” is more visible for small values of N when, for sufficiently small confining radii, P_{3_1} is a non-monotonic curve with one maximum. As the confinement radius R is further reduced, P_{3_1} decreases in favour of more compact conformations. For longer polymers ($N > 125$) the maximum becomes progressively less evident and we observe a shoulder for small values of $1/R$, that disappears for $N = 400$. The possibility that the probability of trefoil knots also obeys a scaling law has not (to our knowledge) been investigated before. Fig. 7 displays the data of trefoil probabilities plotted as a function of the same scaling variable obtained for the unknot. The data, which pertain only to lengths $250 \leq N \leq 450$ (since shorter rings display the above mentioned “peak” or shoulder) appear well collapsed. The optimal collapse of the trefoil data is obtained for an exponent $\alpha \simeq 2.3$ somewhat larger than for the unknot (but the trefoil data pertains to fewer ring lengths than for the unknot). The results therefore indicate that, for sufficiently large N , the trefoil probabilities also obey a scaling law with an exponent that may be the same as that of the unknots.

Figs. 4c,d,e and 5c,d,e and show plots analogous to the one in figs.4b and 5b but now refer to the probability of forming 4, 5 and 6 crossing knots respectively. The trend observed for the trefoil knot is also observed for the other prime knots considered here. Indeed, all the curves for short polymers (small N) have a maximum as a function of the inverse radius, while those for longer polymers decrease monotonically with $1/R$. It is interesting to observe that for polymers with N up to 200, the confinement eventually forces the 5 crossing knots to outnumber the 4_1 knots, which are more numerous in the unconstrained case ($R = \infty$). This result is consistent with what observed in Ref. [11] for shorter random rings. This effect is illustrated in Fig. 8 which clarifies how the confining radius corresponding to the crossover from 4 to 5 crossing knots increases for increasing length N .

Also the case of knots with 6 minimal crossings is particularly interesting since there are two chiral knots (6_1 and 6_2) and one achiral knot (6_3). The study of the relative fraction of the chiral and achiral 6 crossing knots shows the effect of confinement on the chirality of knots. Fig. 9 portrays the occurrence probability of 6_1 , 6_2 and 6_3 as a function of $1/R$ for 3 different values of N . As one can see, the least probable knot is the achiral one whose relative population among the 6 crossing knots, within the explored ranges of N , remains around 25% as confinement is increased. This illustrates that, in this simple case, confinement alone is not sufficient to induce the chiral bias that is encountered in the above-mentioned biological contexts.

In general, we find that the probability of formation of a given knot type increases with $1/R$ –

with respect to its unconstrained value – only if the chain length is small enough, specifically below the length that maximises the probability of formation of that knot type [34]. As the confinement radius R decreases we expect that the complexity of the knots present in the ring would increase. This complexity can be manifested either with the formation of prime knots with large minimal crossing number or with the occurrence of composite knots, i.e., knots that are connected sums of prime knots. It is therefore interesting to monitor how the relative fraction of composite/prime knots depends on R .

Figs. 4f and 5f show the probabilities of forming a composite knot [21] for random chains of different lengths. The trend follows the expectation that as confinement increases the fraction of composite knots becomes higher.

Fig. 10 shows a 'phase diagram' showing what knot class is most populated. Throughout the values of the parameters $(N, 1/R)$ considered here, the most populated class was either the unknot or the composite knots. As N and $1/R$ increase, i.e. as one moves to the right and to the top in the parameter space in Fig. 10, knots become increasingly complex and prime knots occur less and less often. Fig. 10b shows the phase diagram restricted to the ensemble of prime knots alone.

IV. WRITHE

Up to now we have focused on the topological properties of the system but it is also useful to have geometric measures of the polymer entanglement. One interesting geometric property is the *writhe* of the polymer, which has been proved to be useful in modelling the degree of supercoiling in DNA[35, 36]. To define writhe consider any oriented simple closed curve in \mathcal{R}^3 , and project it onto \mathcal{R}^2 in some direction \hat{x} . In general, the projection will have crossings and, for almost all projection directions, these crossings will be transverse, so that we can associate a sign $+1$ or -1 to each crossing as in Fig. 11. The sign of a crossing is independent of curve orientation, because changing the curve orientation changes the orientation of both segments involved in a crossing in a projection. For this projection we form the sum of these signed crossing numbers, $S(\hat{x})$, and then average over all projection directions \hat{x} . This average quantity is the writhe wr of the curve[37]. If we compute the writhe of each configuration with N segments, and average over the set of configurations, clearly the expected value of the writhe, $\langle wr \rangle$, is zero by symmetry. Consequently, we shall be interested in the expectation of the absolute value of the writhe, $\langle |wr| \rangle$, or the expectation of its square, $\langle wr^2 \rangle$ (or, more generally, in the distribution of wr). The primary difficulty with

the computation of the writhe is that it involves averaging the sum of signed crossing numbers over all projection directions. For polygons on the cubic lattice the calculation of writhe is greatly simplified by a theorem[38, 39] which reduces the writhe computation to the average of linking numbers of the given curve with four selected push-offs. Unfortunately this result is not applicable here and we have to rely on the natural definition of the writhe that we estimate by averaging $S(\hat{x})$ over more than 500 random projections (\hat{x}). Note that the writhe distribution before and after the smoothing differ considerably (as should be expected and consistently with lattice calculations [13]). The data on the writhe presented here refer to the situation before smoothing.

The reweighting technique can be used to calculate the fraction of conformations of given writhe, wr , that can fit inside a sphere of radius, R , $W_N(wr, R)$. By necessity this can be accomplished only after introducing a discretization of the values for the writhe. The reweighting method therefore provides directly the fundamental quantity of our interest, that is the probability distribution for the writhe of rings of given lengths that fit in hulls of given radius. From this fundamental quantity all the moments of the distribution, including the averages $\langle wr \rangle$ and $\langle wr^2 \rangle$ can be calculated:

$$\langle wr_N(R)^k \rangle = \frac{\int_{-\infty}^{+\infty} dwr wr^k W_N(wr, R)}{\int_{-\infty}^{+\infty} dwr W_N(wr, R)} \quad (6)$$

As far as the writhe is concerned we wish to elucidate two features that have not been previously addressed in off-lattice contexts. The first one pertains to how, at given N , the probability distribution for the writhe changes as rings are confined in tighter spaces while the second concerns the N dependence of the expectation of the absolute value of the writhe for confined rings.

Fig. 12 shows the (normalized) probability distribution of the writhe for different values of R and N . One can notice that, for fixed N , as the confining sphere decreases, the writhe distribution becomes broader and broader keeping their averages equal to zero (as it should be since we are considering the whole set of rings). For any given R the width of such distributions can be measured, for example, by computing the mean of the absolute value of the writhe $\langle |wr_N(R)| \rangle$. It is known that in the unconstrained case, $R = \infty$, the writhe spread is proportional to \sqrt{N} [40]. Accordingly, the ratio $\langle |wr_N(R = \infty)| \rangle / \sqrt{N}$ will be independent of N . To check if this simple scaling behaviour holds also for finite values of R , we have considered the quantity $\log[\langle |wr_N(R)| \rangle / \sqrt{N}]$, which is reported in Fig. 13. As expected, the curves take on the same value for $1/R \rightarrow 0$. This collapse does not extend, however, for finite R 's. The tendency towards linear behaviour that is visible for sufficiently large $1/R$ (i.e. for strong confinement) is suggestive of an exponential

dependence of the writhe on $1/R$ for all values of N .

The second feature we wish to elucidate is if and how the N dependence of the absolute value of the writhe, is affected by the confinement. For unconstrained polygons on the cubic lattice rigorous arguments have shown that $\langle |wr| \rangle$ cannot grow slower than \sqrt{N} [40] and numerical results gives a power law behavior $\langle |wr| \rangle \sim N^\alpha$ with $\alpha \sim 0.52 \pm 0.04$ [40]. To the best of our knowledge no such investigations have been carried out for the case of confined polymer rings, though it has been argued that for highly compact conformations of a simple closed curve the writhe increases like $N^{4/3}$ [41]. In Fig 14 a log-log plot of $\langle |wr| \rangle$ vs N is reported for the unconstrained case (lower curve) and for rings of different length but confined in a sphere with the same radius. Both curves appear to follow a power law behavior. A linear regression in the log-log plot gives an exponent equal to 0.498 ± 0.002 for the $R = \infty$ case, in excellent agreement with what is expected for unconstrained rings. For the particular choice of confining radius of Fig. 14, instead, the exponent is approximately 0.75, strikingly different from the square root behavior. Indeed, the deviations from the $R = \infty$ behaviour appear to increase as a function of confinement. This is in accord with the intuitive expectation that confinement can dramatically increases the geometrical complexity of the rings, and hence impact on their writhe. The linear trend of the finite- R data of Fig. 14 is suggestive of the existence of R -dependent scaling laws for $\langle |wr_N(R)| \rangle$ as a function of N . To reach a definite conclusion about the existence of such peculiar scaling behaviour it would be necessary to extend significantly the range of values of N to be explored.

V. DISCUSSION AND CONCLUSIONS

We investigated the occurrence of various types of knots in random rings subject to spatial confinement. The sampling of ring conformations was carried out within a multiple Markov chain strategy. The correct identification of knotted conformations was aided by a hierarchical simplification of the ring conformations by first smoothing and shrinking the rings and then applying the operations and calculations of KnotFind to their two-dimensional projections.

The fraction of composite knots is shown to increase significantly with both their length, N , and the inverse radius of the confining sphere, $1/R$. Indeed, in tightly confined geometries the majority of knots are composite. Furthermore, the probability of occurrence for the simplest prime knots displays a non-monotonic behaviour: the initial increase with confinement is followed by a subsequent decay at still higher compression. This trend is similar to that observed for unconstrained

random knots for increasing length.

The scaling behaviour of the unknotting probability was also investigated. Owing to the powerful numerical strategy adopted here, we improve a previous estimate of the exponent governing the scaling dependence on N and $1/R$. Finally, the analysis of the writhe distribution at fixed ring length suggests an exponential broadening of the distribution under strong confinement. Also, if N is increased at fixed R it is found that the writhe distribution width increases more rapidly than in the case of unconfined knots.

Despite the fact that the rings considered here are not subject to volume exclusion interaction it is pleasing that the observed increase of the knotting probability with confinement is in line with the experimental findings on DNA [6, 11]. It is our intention, for the future, to go beyond this significant qualitative agreement and consider the more realistic case of rings with volume exclusion. Indeed previous results [2, 42] suggest that without confinement ($R = \infty$), for a fixed N the knot probability is very sensitive to volume exclusion – as one increases the volume of the segments, the knot probability decreases very quickly. The algorithm employed here ought to be efficient also for the sampling of confined rings with excluded volume, though we can envisage that the increased computational complexity will prevent us from attaining the same ring lengths or degree of confinement obtained here.

This work was funded by INFM. DWS was partially supported by a Burroughs Wellcome Fund Interfaces grant to the Program in Mathematics and Molecular Biology. CM and DWS acknowledge the hospitality of the Institut des Hautes Etudes Scientifiques in Bures-sur-Yvette where part of this study was undertaken. We are grateful to Ken Millet, Eric Rawdon, Andrzej Stasiak and Tommaso Zillio for useful discussions and comments.

-
- [1] A. V. Vologodskii, N. J. Crisona, B. Laurie, P. Pieranski, V. Katritch, J. Dubochet, A. Stasiak, *J. Mol. Biol.* **278**, 1 (1998).
 - [2] V. V. Rybenkov, N. R. Cozzarelli, A. V. Vologodski, *Proc. Natl. Acad. Sci. USA* **90**, 5307 (1993).
 - [3] A. Bucka, A. Stasiak, *Nucl. Acid Res.* **30**, e24 (2002).
 - [4] J. Yan, M. O. Magnasco, J. F. Marko, *Nature* **401**, 932 (1999).
 - [5] S. Trigueros, J. Salceda, I. Bermudez, X. Fernandez, J. Roca, *J. Mol. Biol.* **335** 723 (2004).
 - [6] J. Arsuaga, M. Vazquez, S. Trigueros, D.W. Sumners, and J. Roca, *Proc. Nat. Acad. Sci.* **99**, 5373

- (2002).
- [7] S. Trigueros, J. Arsuaga, M.E. Vazquez, D.W. Sumners and J. Roca, *Nucleic Acids Res.* **29**, 67 (2001).
 - [8] J. Arsuaga, R. K. Z. Tan, M. Vazquez, D. W. Sumners, S. C. Harvey, *Biophys. Chem.* **101**, (2002) 475.
 - [9] J. C. LaMarque, T. V. L. Le, S. C. Harvey, *Biopolymers* **73**, 348 (2004).
 - [10] D. Marenduzzo, C. Micheletti, *J. Mol. Biol.* **330**, 485 (2003).
 - [11] J. Arsuaga, M. Vazquez, P. McGuirk, S. Trigueros, D. W. Sumners, J. Roca, *Proc. Nat. Acad. Sci.* **102**, 9165 (2005).
 - [12] J.P.J. Michels, F.W. Wiegel, *Proc. Roy. Soc. A* **403**, 269 (1986).
 - [13] M. C. Tesi, E. J. Janse van Rensburg, E. Orlandini, S. G. Whittington, *J. Phys. A* **27**, 347 (1994).
 - [14] M.L. Mansfield, *Macromolecules* **27**, 5924 (1994).
 - [15] C. Micheletti and D. Marenduzzo, in *Physical and Numerical Models in Knot Theory* Calvo, Rawdon and Stasiak Editors, World Scientific Press, Singapore (2005).
 - [16] C. Micheletti, V. De Filippis, A. Maritan and F. Seno, *Proteins*, **53**, 720 (2003).
 - [17] K.C. Millett, in *Physical knots: knotting, linking and folding geometric objects in R^3* , Contemporary Math 304, (2001)
 - [18] M. C. Tesi, E. J. Janse van Rensburg, E. Orlandini, S. G. Whittington, *J. Stat. Phys.* **29**, 2451 (1996).
 - [19] K. Koniaris, M. Muthukumar, *J. Chem. Phys.* **95**, 2873 (1991).
 - [20] W. R. Taylor, *Nature* **406**, 916 (2000).
 - [21] C. C. Adams, *The knot book*, (W.H. Freeman and Company, New York 1994) .
 - [22] C. H. Dowker, M. B. Thistlethwaite, *Topology Appl.* **16**, 19 (1983).
 - [23] Knotfind is a routine implemented in the KnotScape package created by Jim Hoste and Morwen Thistlethwaite. See for example www.math.utk.edu/~morwen/knotscape.html.
 - [24] V. Katrich, W. K. Olson, A. Volodogskii, J. Dubochet, A. Stasiak, *Phys. Rev. E* **61**, 5545 (2000).
 - [25] A. Dobay, J. Dubochet, K. Millett, P. E. Sottas, A. Stasiak, *Proc. Natl. Acad. Sci USA* **100**, 5611 (2003).
 - [26] K.C. Millett and E.J. rawdon in *Physical and numerical models in knot theory*, Calvo, Millett, Rawdon and Stasiak eds., World Scientific, Singapore, (2005). *Disc. Appl. Math.* **25**, 273 (1989).
 - [27] T. Deguchi and K. Tsurusaki, *Phys. Rev E* **55**, 6245 (1997).
 - [28] D. W. Sumners, S. G. Whittington, *J. Phys. A* **21**, 1689 (1988).
 - [29] N. Pippenger, *Disc. Appl. Math.* **25**, 273 (1989).
 - [30] Y. Diao, N. Pippenger, D.W. Sumners, *J. Knot Theory and Ramifications* **3**, 419 (1994).

- [31] Y. Diao, *J. Knot Theory and Ramifications* **4**, 189 (1995).
- [32] S. M. Bhattacharjee, F. Seno, *J. Phys. A* **34**, 6375 (2001).
- [33] T. Zillio, I. Volkov, J. R. Banavar, S. P. Hubbell, A. Maritan, *Phys. Rev. Lett.* **95**, 098101 (2005).
- [34] A. Dobay, P.-E. Sottas, J. Dubochet, A. Stasiak, *Lett. Math. Phys.* **55**, 239 (2001).
- [35] W.R. Bauer, F.H. C. Crick, J. H. White, *Sci. American* **243**, 118 (1980).
- [36] J.H. White, W.R. Bauer, *J. Mol. Biol.* **189**, 329 (1986).
- [37] F.B. Fuller, *Proc. Natl. Acad. Sci. USA*, **68**, 815 (1971).
- [38] R.C. Lacher, D.W Sumners, *Data structures and algorithms for the computation of invariants of entanglements: links, twist and writhe*, in *Computer Simulations of Polymers*, ed. R.J. Row (Englewood Cliffs. NJ: Prentice-Hall) 365 (1991).
- [39] E.J. Janse van Rensburg, E. Orlandini, D.W. Sumners, M.C. Tesi, S.G. Whittington, *J. Knot Theory and Its Ramifications* **6**, 31 (1997).
- [40] E.J. Janse van Rensburg, E. Orlandini, D.W. Sumners, M.C. Tesi, S.G. Whittington, *J.Phys. A* **26**, L981 (1993).
- [41] J. Cantarella, D. DeTurk and H. Gluck, *Upper bounds for the writhing of knots and the helicity of the vector fields*, Proceedings of the Conference in Honor of the 70th Birthday of Joan Birman Jane Gilman, Xiao-Song Lin, William Menasco (eds) International Press, AMS/IP Series on Advanced Mathematics (2000).
- [42] K. V. Klenin, A. V. Vologodskii, V. V. Anshelevich, A. M. Dykhne, M. D. Frank-Kamenetskii, *J. Biomol. Struct. Dyn.* **5**, 1173 (1988).

Figure Captions

Figure 1: Example of configurations at four stages of the smoothing procedure of two rings of 100 links. a-d refer to an unknot while e-h to a trefoil knot.

Figure 2: Probability of unknown knots as a function of N .

Figure 3: Length dependence of the probability of occurrence of various types of knots in unconstrained random rings ($R = \infty$, the number of crossing is indicated in the legend). The dashed line is the single exponential fit through the unknot data, yielding a decay exponent equal to $b = 0.0041 \pm 0.0001$ (see text).

Figure 4: Probabilities of formation of various types of knots of $N = \{100, 200, 300, 400\}$ segments as a function of the inverse radius of the enclosing sphere, $1/R$. Open symbols denote the region when the fraction of unknown knots exceeds 10% (but is smaller than 50%). No data is plotted in the region when the fraction of unknown knots exceeded 50%. The plots refer to knots of type: (a) unknot, (b) 3_1 , (c) 4_1 , (d) 5_1 and 5_2 , (e) 6_1 , 6_2 and 6_3 and (f) composite.

Figure 5: Probabilities of formation of various types of knots as a function of the ring length N and inverse radius of the enclosing sphere, $1/R$. At values of $1/R$ greater than those indicated with the red line, the observed fraction of unknown knots exceeded 10% (but is smaller than 50%). No data is plotted in the region when the fraction of unknown knots exceeded 50%. The plots refer to knots of type: (a) unknot, (b) 3_1 , (c) 4_1 , (d) 5_1 and 5_2 , (e) 6_1 , 6_2 and 6_3 and (f) composite.

Figure 6: Scaling of the unknotting probabilities for a random rings with number of segments ranging from 100 to 450 in steps of 25.

Figure 7: Scaling of the trefoil probabilities for a random chain with N from 250 to 450 in steps of 25.

Figure 8: The plot shows the length of the rings, N , above which the $k = 5$ knots outnumber

the $K = 4$ ones.

Figure 9: Dependence on confining radius of the probability of forming a $6_{1,2,3}$ knot of $N = \{100, 200, 300\}$ segments.

Figure 10: (a) “Phase diagram” showing, for each point in the $(N, 1/R)$ plane considered in the simulations, what is the most populated class of knots. In panel (b) the diagram is restricted to the class of prime knots alone. The dashed line indicates the threshold between trefoil and more complex knots, but it has been computed in a region where the unclassified knots are the majority.

Figure 11: Positive and negative crossings are determined by a right-hand rule.

Figure 12: Probability distribution for the writhe. Each figure corresponds to a fixed value of N (top: $N = 100$, middle $N = 200$ and bottom $N = 300$) and different curves correspond to different R values.

Figure 13: Dependence of the logarithm of $\langle |wr| \rangle / \sqrt{(N)}$ on $1/R$. Different curves correspond to different values of N .

Figure 14: Log-log plot of the absolute value of the writhe as a function of the ring length, N . The two data sets corresponds to the unconstrained case (black circles) and to polymer rings confined in a sphere of inverse radius $1/R = 0.226$ (squares).

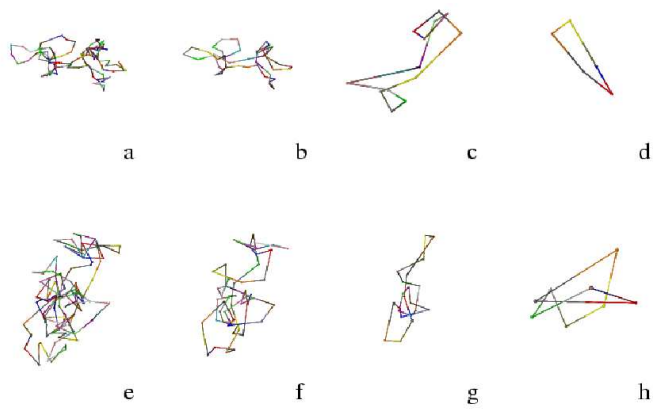


FIG. 1:

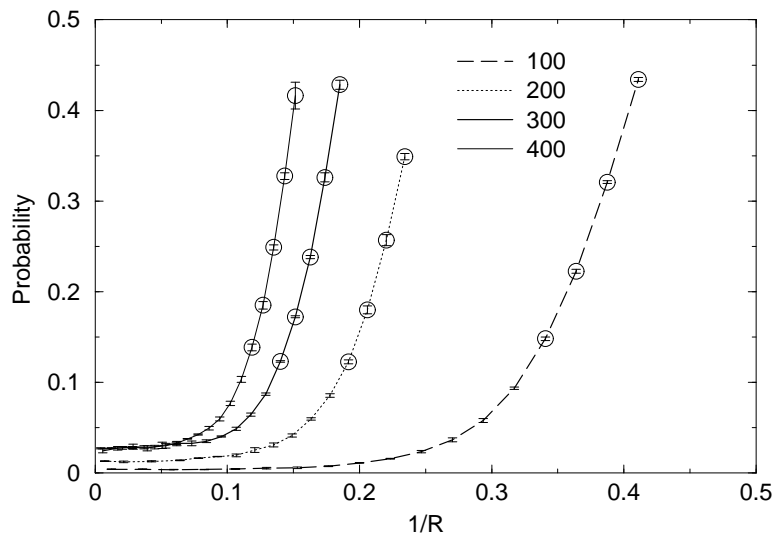


FIG. 2:

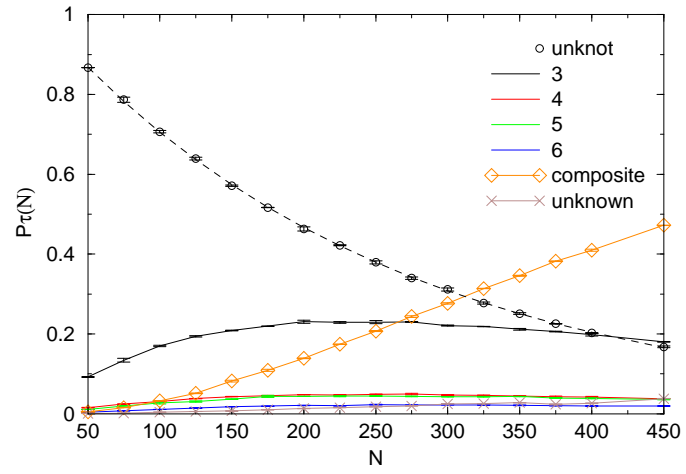


FIG. 3:

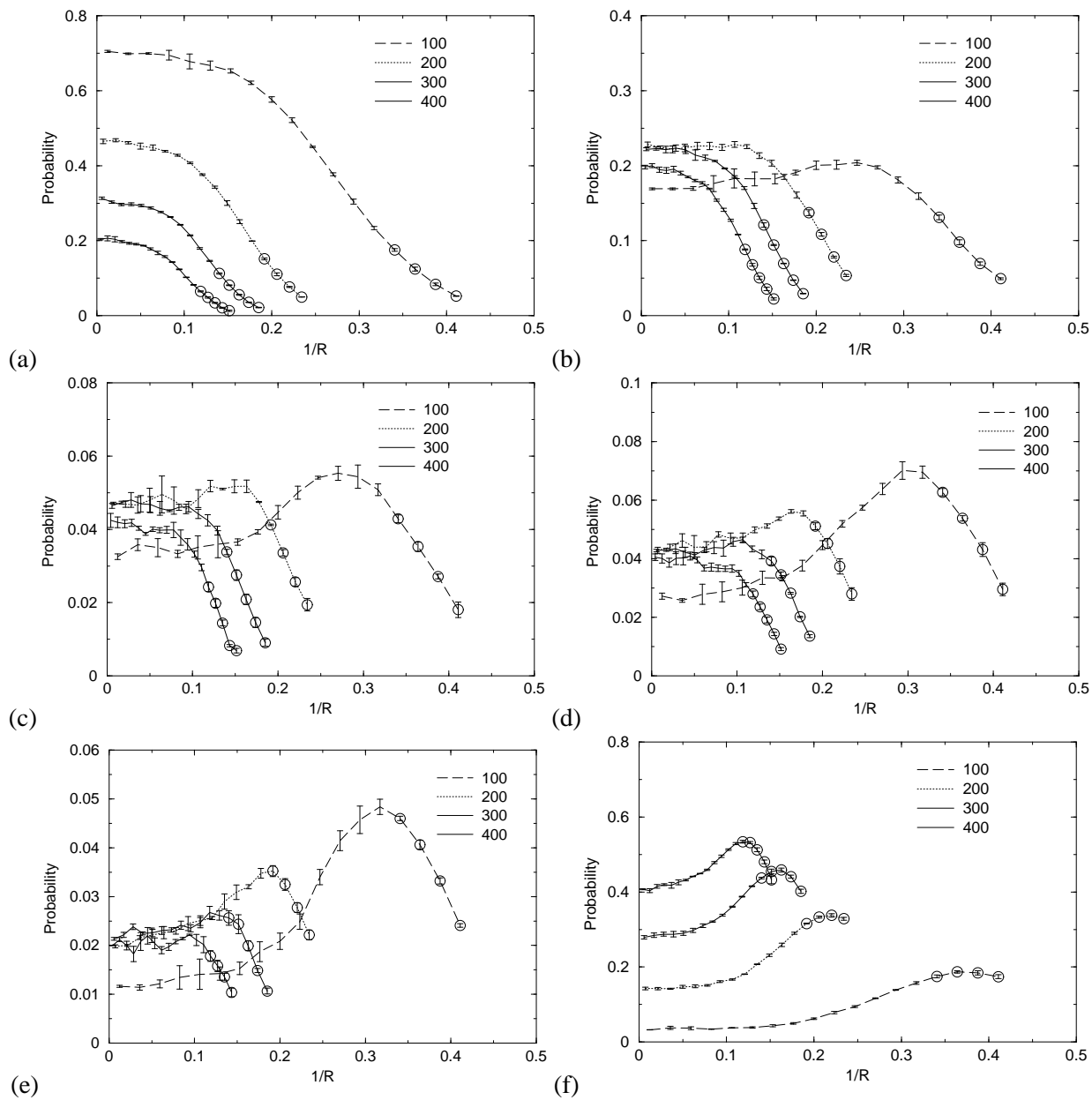
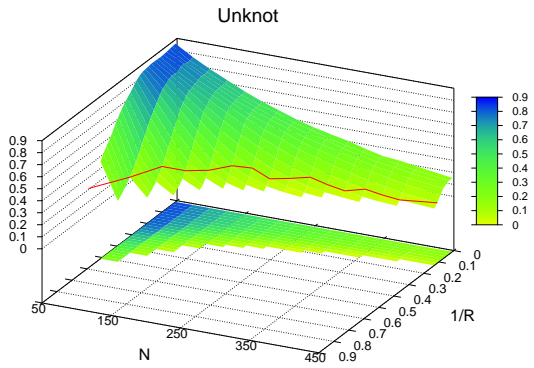
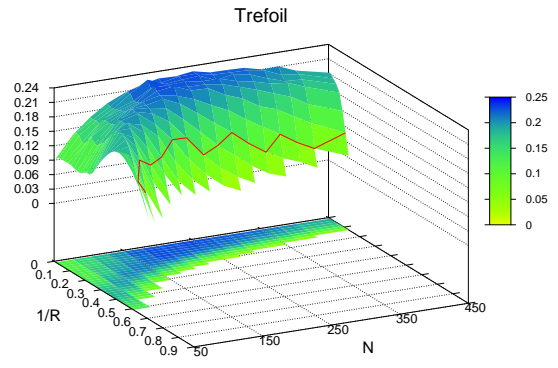


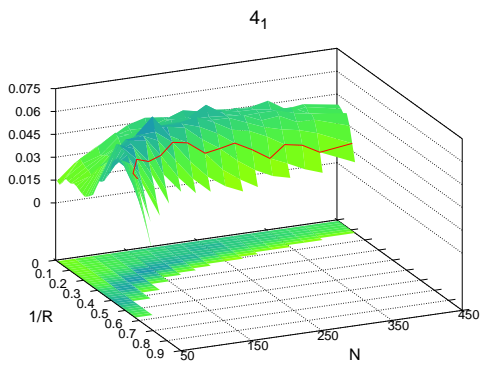
FIG. 4:



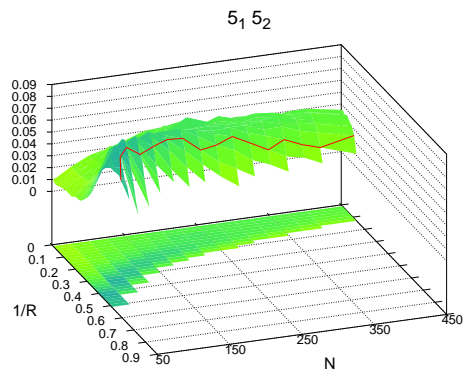
(a)



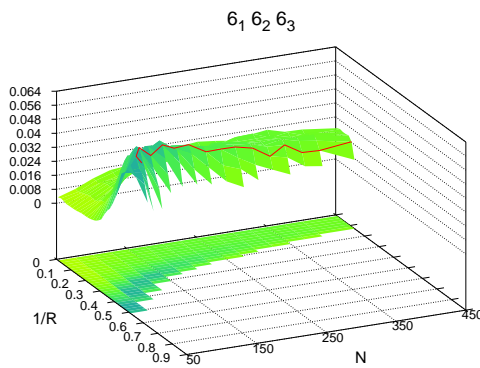
(b)



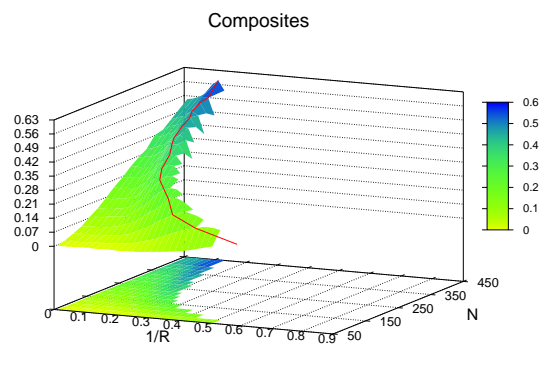
(c)



(d)



(e)



(f)

FIG. 5:

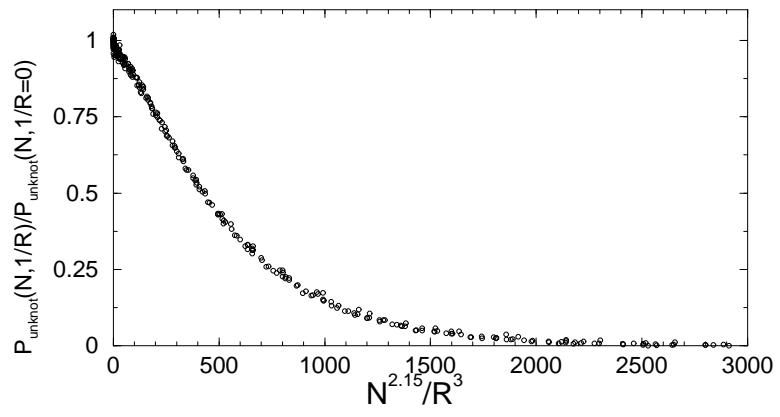


FIG. 6:

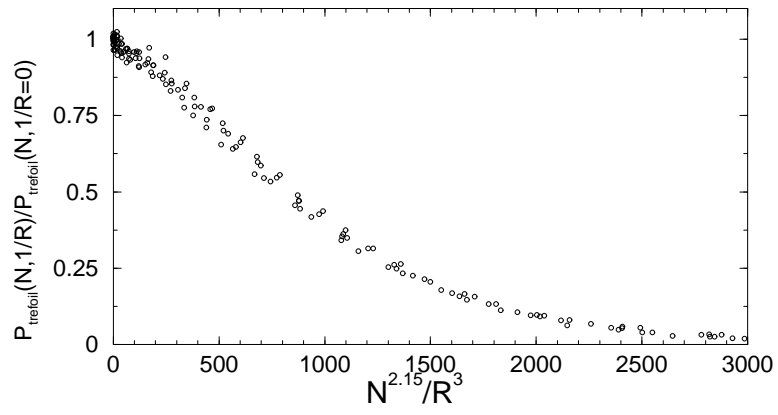


FIG. 7:

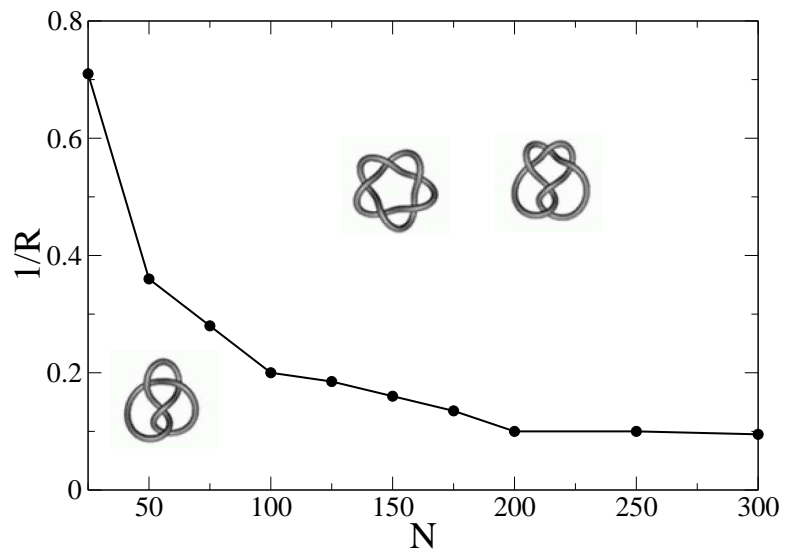


FIG. 8:

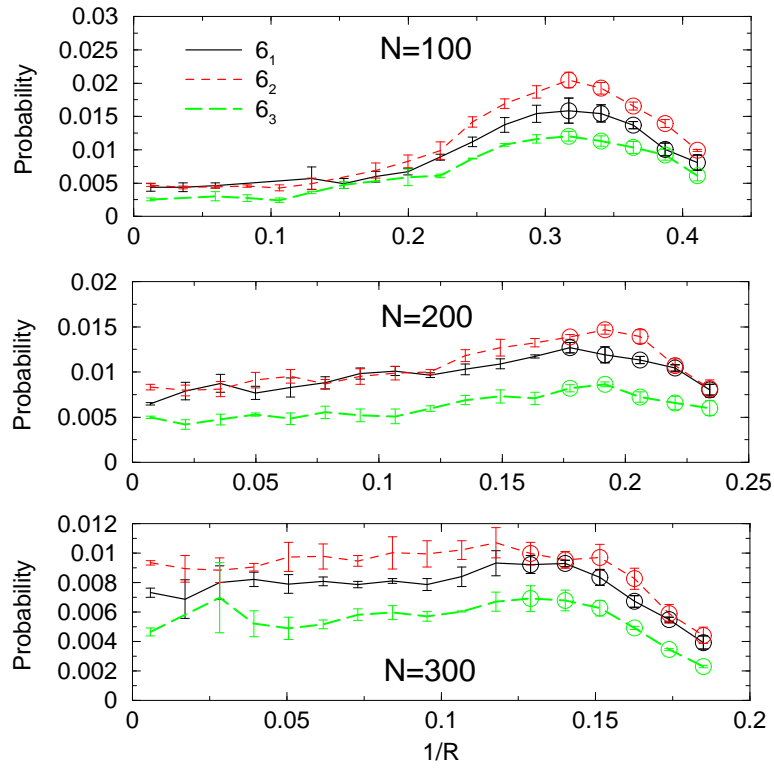


FIG. 9:

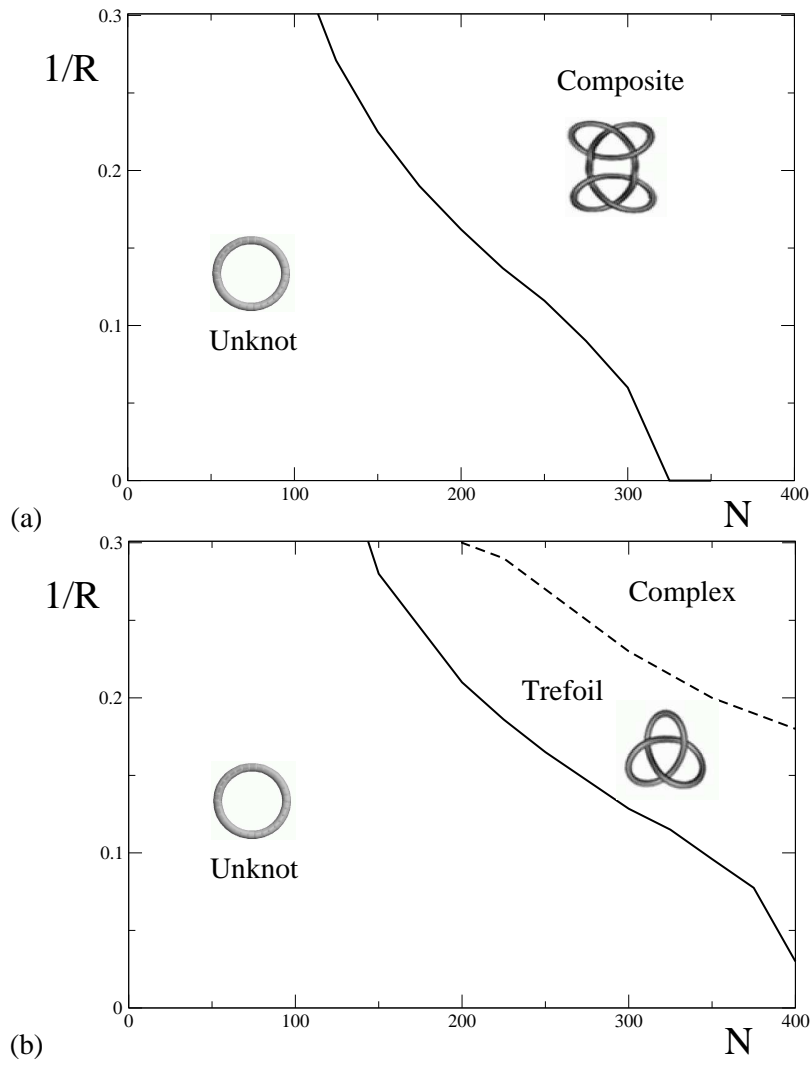


FIG. 10:

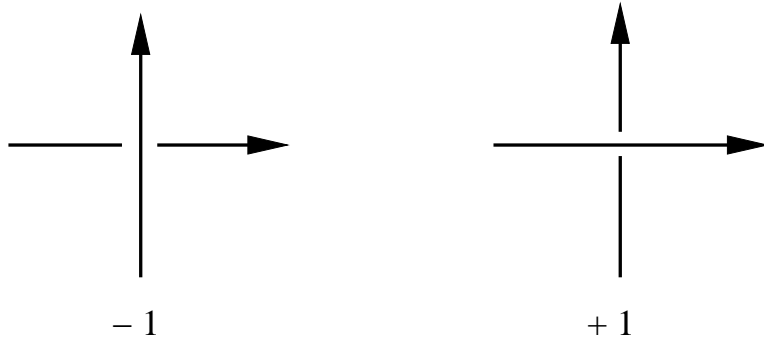


FIG. 11:

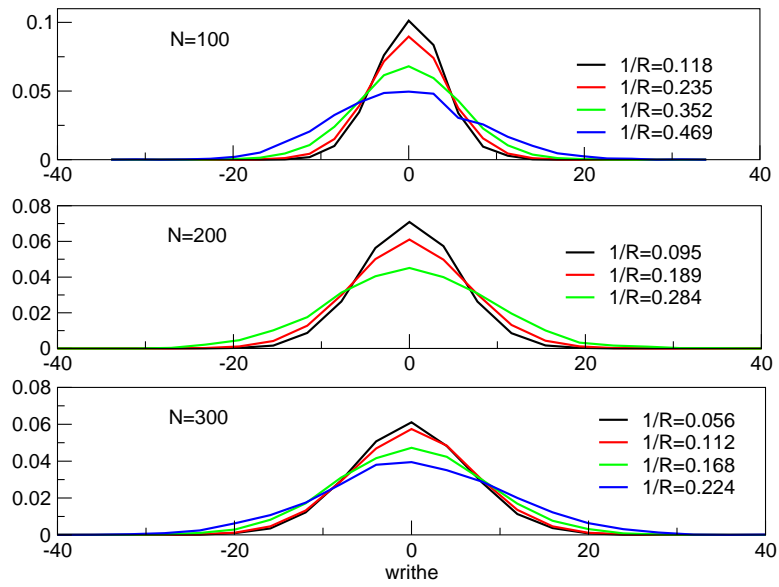


FIG. 12:

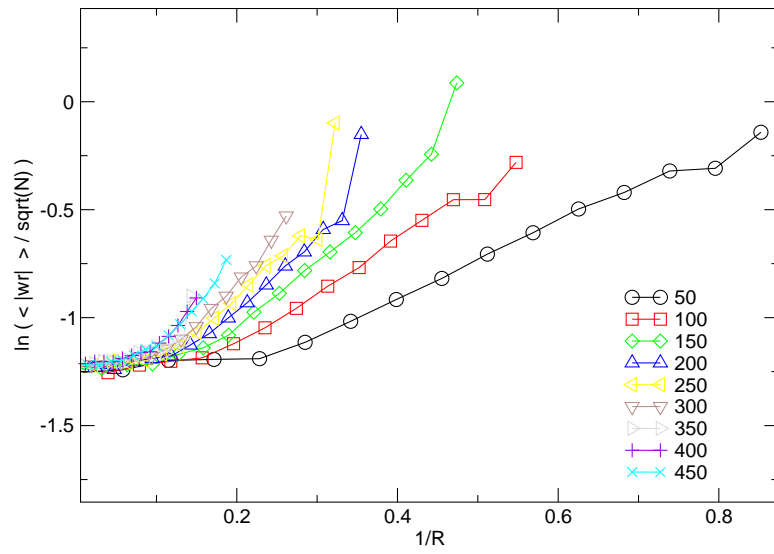


FIG. 13:

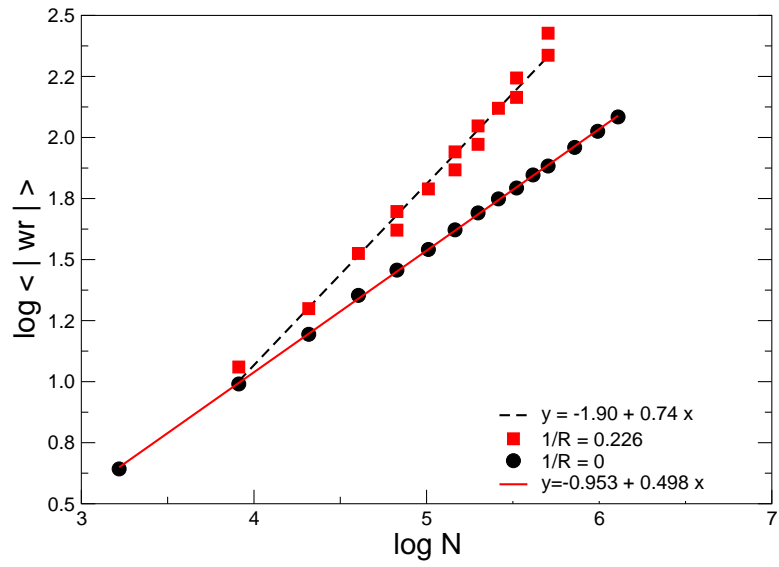


FIG. 14: